Long-streamer travel-time tomography of the shallow Porcupine Basin reveals across-axis variations in petrophysical properties

Prada, M.[1,2] *, Lavoué, F.[1,2], Saqab, M.M.[1,3], O'Reilly, B. M.[1,2], Lebedev, S.[1,2]

[1] Irish Centre for Research in Applied Geosciences (iCRAG). [2] Dublin Institute for Advanced Studies (DIAS), Geophysics Section, 5 Merrion Square, Dublin 2, Ireland.
[3] School of Earth Sciences, University College Dublin, Belfield, Ireland. ****mprada@cp.dias.ie***

I. Introduction

The aim this study is to interrogate petrophysical parameters such as porosity (ϕ) across the axis of the shallow Porcupine Basin to assess the potential presence of fluids. Understanding of the distribution of fluids and characterization of potential overpressured areas within the basin can contribute to drilling and environmental derisking during exploration of offshore resources.

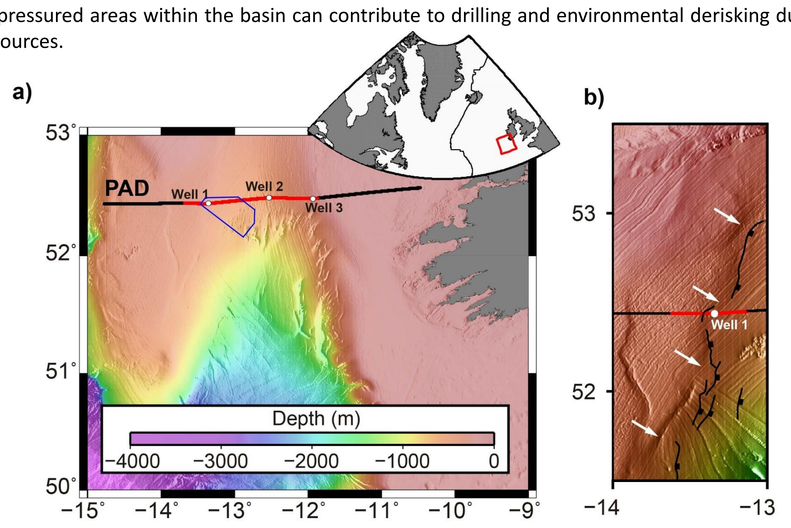

Figure 1.- (a) Bathymetry map of the Porcupine Basin showing the location of the MCS line PAD (black line). Only shot gathers along the red section are included in this study to perform the travel-time tomography of streamer data. White dots are exploration wells used in this study. The blue polygon depicts the location of the 3D seismic data (Worthington and Walsh, 2016) used to assess. **(b)** Close-up of the bathymetry map at the western margin of the Porcupine Basin showing the location of Mesozoic basement fault system from Worthington and Walsh (2016). White arrows point at a subtle step in the bathymetry potentially attributed to this later fault system. The red section is the location of Fig. 9.

II. Data & Picking

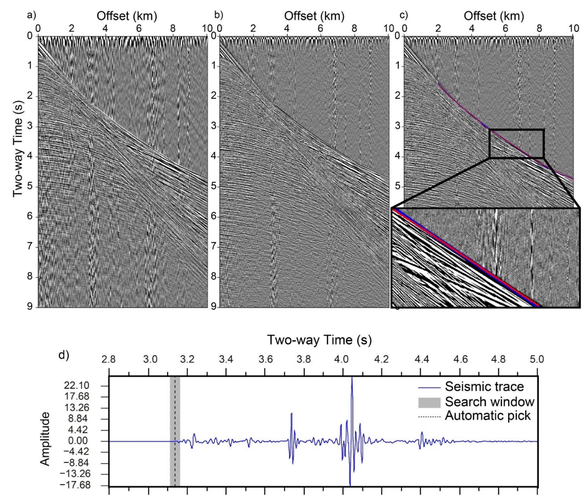

Figure 2.- (a) Shot gather along line PAD filtered using a bandpass filter (3-100 Hz), and **(b)** convolved with a user-defined filter derived from the direct wave. **(c)** Same shot gather showing the automatically picked travel-times using Kurtosis (Saragiotis et al., 2002) (in blue), and synthetic travel-times after the inversion (in red). **(d)** Seismic trace from the same shot gather showing the automatically selected travel-time of the first arrival (dashed line). The grey area shows the search window in which the Kurtosis-based automatic picker is restricted.

III. 2D V_p model

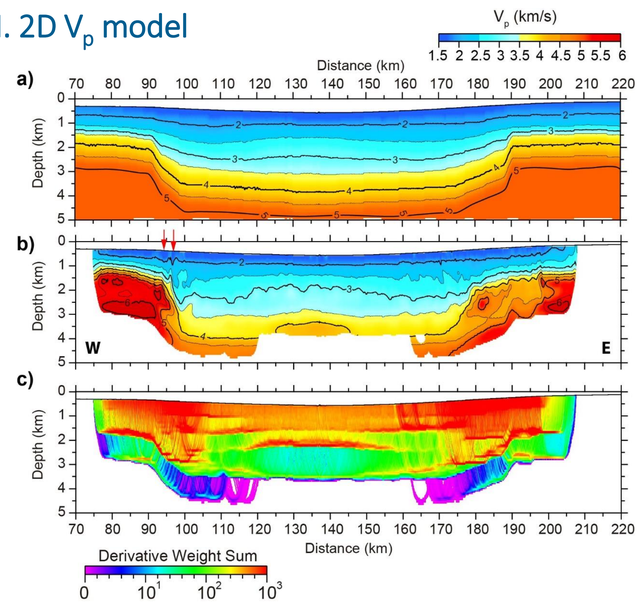

Figure 3.- (a) Starting V_p model. **(b)** Preferred tomographic model showing the velocity structure resolved by the inversion using TOMO2D software adapted to streamer data (Begović et al., 2017). This model is used as starting model in the full waveform inversion **(see poster from F. Lavoué et al.,).** Red arrows show the location of both low velocity anomalies assessed in the resolution analysis in Fig. 6. **(c)** Derivative weight sum of the final tomographic model. This image can be taken as a proxy of the ray coverage through the model.

IV. Integration of time-migrated MCS data

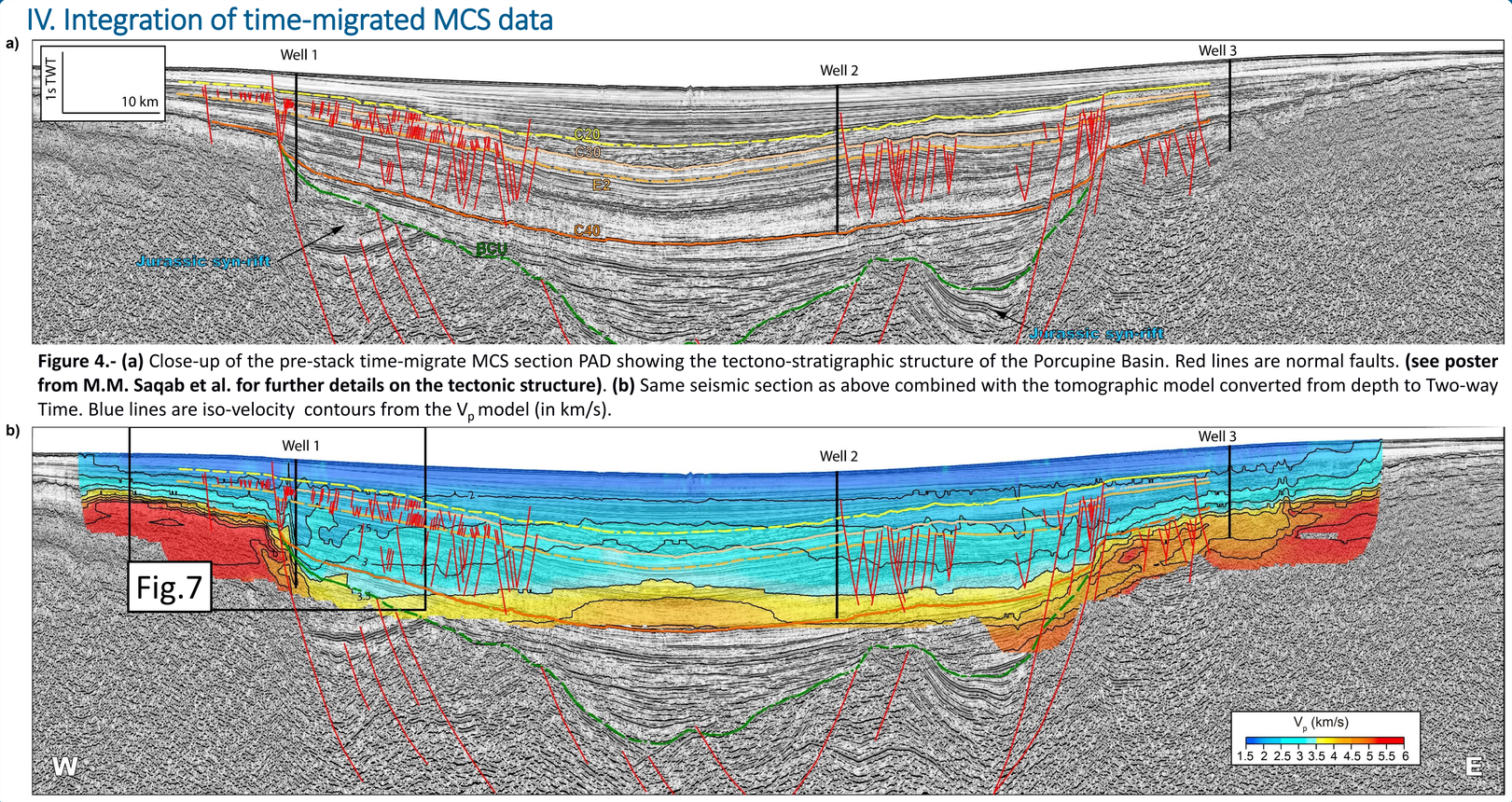

Figure 4.- (a) Close-up of the pre-stack time-migrate MCS section PAD showing the tectono-stratigraphic structure of the Porcupine Basin. Red lines are normal faults. **(see poster from M.M. Saqab et al. for further details on the tectonic structure)**. **(b)** Same seismic section as above combined with the tomographic model converted from depth to Two-way Time. Blue lines are iso-velocity contours from the V_p model (in km/s).

V. Uncertainty & Resolution analysis

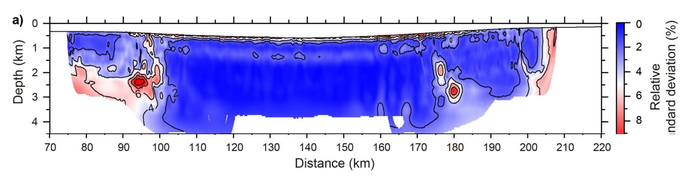

Figure 5.- (a) Relative standard deviation respect the final velocity model resulting from the Monte Carlo analysis.

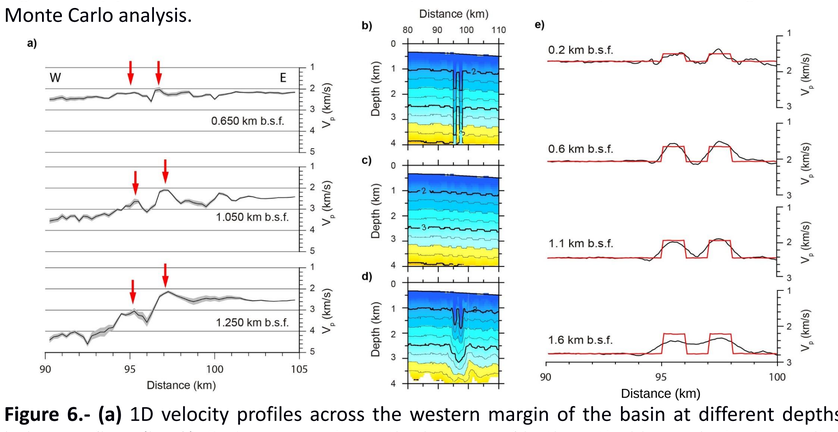

Figure 6.- (a) 1D velocity profiles across the western margin of the basin at different depths below seafloor (b.s.f.). Red arrows point at the location of both vertical low-velocity anomalies indicated in Fig. 3b. The grey area represents the error bar inferred from the Monte Carlo analysis, while the black line is the average V_p estimate. **(b-d)** Synthetic test showing the retrieval of two 1-km-wide anomalies. **(b)** Target model, **(c)** starting model, and **(d)** final model **(e)** Horizontal 1D V_p profiles extracted across both anomalies at different depths below seafloor. The red line is the velocity profile across the target model, while the black line shows the retrieved velocity structure.

VI. Integration of 3D data

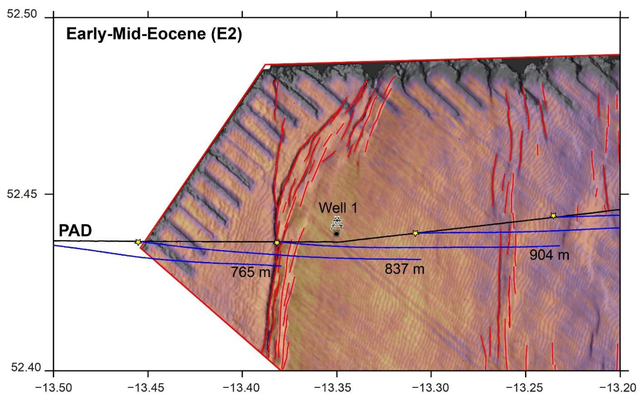

Figure 7.- 3D surface map of the Early-Mid-Eocene E2 horizon from the 3D seismic data set mentioned in Fig.1a, together with the location of Well 1 and line PAD. The blue lines represent the feathering of the streamer and the values at the edge of each line show the total amount of drifting respect the location of line PAD. Yellow stars are source points. Red lines are normal faults. **(see poster from M.M. Saqab et al. for further details on the tectonic structure).** The lack of normal faulting within the feathering of the streamer near Well 1 makes difficult to explain both elongated low-velocity anomalies observed in the hanging wall in Fig. 4b by three-dimensional effects caused by out-of-plane structures.

VII. V_p, density, porosity from Well data

Figure 8.- (a) Bulk density measurements vs sonic log measurements from Wells 1, 2 and 3. The red line is the polynomial function that satisfies the distribution of measurements (R^2~0.7). **(b)** ϕ model derived from the V_p model using the time-averaged equation from Wyllie et al. (1956) showing the region where ϕ measurements were taken in Well 1 and Well 2. **(c-d)** 1D ϕ -depth profiles comparing ϕ measurements (red dots) with the V_p-derived estimates along each Well (grey band). Error bars are represented by the width of each grey band.

VIII. Remarks: basin-bounding low-velocity anomalies

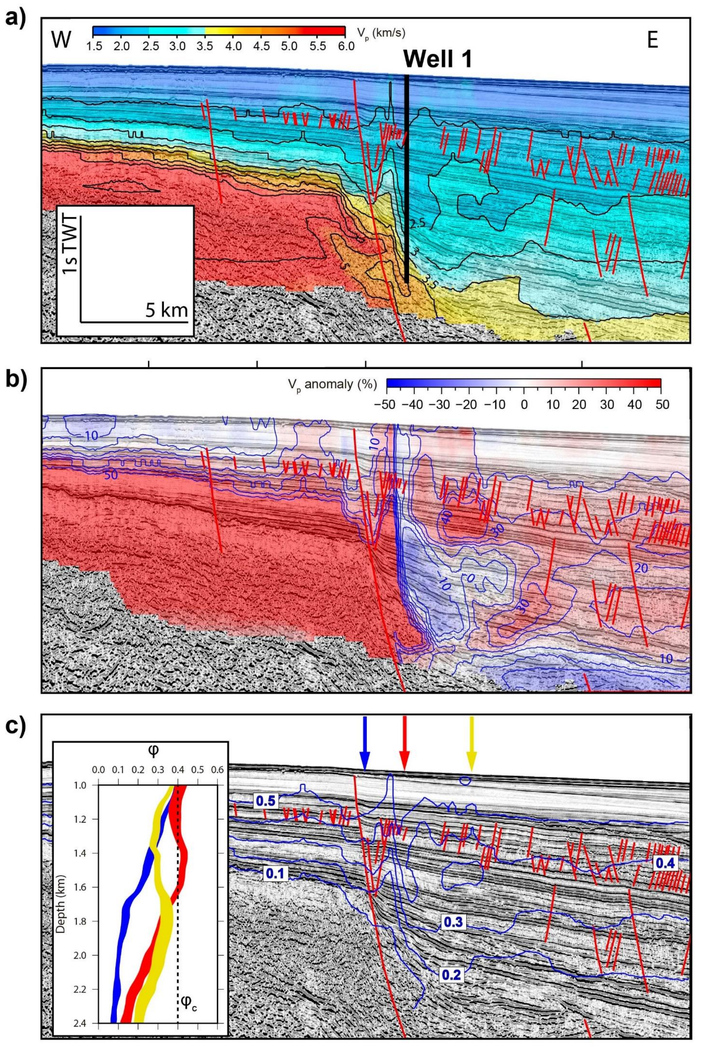

Figure 9.- (a) Close-up of Fig. 4b at the western margin of the Porcupine Basin. Blue lines are iso-velocity contours from the V_p model (in km/s). Red lines are normal faults.

✓ **In the absence of major faulting and three-dimensional effects, the presence of low-velocity anomalies in the hanging wall of the basin-bounding normal fault can potentially be explained by fluid overpressure.**

(b) V_p anomaly obtained from the difference between the starting (Fig. 3a) and the final model (Fig. 3b) overlaying the time-migrated MCS section.

✓ **This image reveals velocities 50 % faster and 10% slower than those used to obtain the time-migrated section.**

(c) ϕ values from Fig. 8b overlaying the MCS section. Coloured vertical arrows show the location of each 1D ϕ -depth profile shown in the ϕ-depth diagram.

✓ **ϕc is critical porosity, above which the strength of the rock drops given that the grains are mostly fluid suspended (e.g. Erickson and Jarrard, 1998). At this range of porosities, deformation is expected to occur at grain-scale over widespread areas (e.g. Wong et al., 1997), which potentially accounts for the lack of normal faults in this particular region of the basin.**

This publication has emanated from research supported in part by a research grant from Science Foundation Ireland (SFI) under Grant Number 13/RC/2092 and co-funded under the European Regional Development Fund and by PIPCO RSG and its member companies.

Ireland's European Structural and Investment Funds Programmes 2014-2020
Co-funded by the Irish Government and the European Union
European Union
European Regional Development Fund
Science Foundation Ireland sfi For what's next

REFERENCES:

Begović, S., A. Meléndez, C. Ranero, & V. Sallarès (2017) Joint refraction and reflection travel-time tomography of multichannel and wide-angle seismic data. EGU General Assembly 2017, Vienna, Austria, Poster EGU2017-17231

Erickson, S. N. & Jarrard, R. D. (1998). Velocity-porosity relationships for water-saturated siliciclastic sediments.*Journal of Geophysical Research: Solid Earth*,*103*(B12), 30385-30406.

Saragiotis, C. D., Hadjileontiadis, L. J., & Panas, S. M. (2002). PAI-S/K: A robust automatic seismic P phase arrival identification scheme. *IEEE Transactions on Geoscience and Remote Sensing*, *40*(6), 1395-1404.

Wong, T. F., David, C., & Zhu, W. (1997). The transition from brittle faulting to cataclastic flow in porous sandstones: Mechanical deformation. *Journal of Geophysical Research: Solid Earth*, *102*(B2), 3009-3025.

Worthington, R. P., & Walsh, J. J. (2016). Timing, growth and structure of a reactivated basin-bounding fault. *Geological Society, London, Special Publications*, *439*, SP439-14.

Wyllie, M. R. 1., Gregory, A. R., and Gardner, L. W., 1956, Elastic wave velocities in heterogeneous and porous media: Geophysics, 21,41-70.

PIP Petroleum Infrastructure Programme